

# Steady-State and Transient Kinetics of Displacement Adsorption and Educt Inhibition in Dehydration of Alcohols on Alumina

VLADIMÍR MORÁVEK

*Institute of Chemical Process Fundamentals, Czechoslovak Academy of Sciences, 165 02 Prague 6, Suchbát, Czechoslovakia*

Received February 28, 1991; revised June 21, 1991

Alumina-catalyzed alkene formation from low aliphatic alcohols has been used as an example of systems showing both Ipatiev displacement adsorption and educt inhibition. The numerically simulated steady-state and the transient kinetic data obtained in the CSTR approximation qualitatively agree with the experimental ones. The Ipatiev–Hinshelwood steady-state and the dynamic models provide close predictions at higher partial pressures of alcohol and under the influence of water in the feed. © 1992 Academic Press, Inc.

## INTRODUCTION

Most of the steady-state kinetic equations for heterogeneous catalytic reactions are based on Langmuir's mode of adsorption, which includes free adsorption sites and a two-step monomolecular exchange (adsorption and desorption) of adsorbed species on them, e.g., Ref. (1). As early as 1913, Ipatiev (2) suggested single-step bimolecular displacement of adsorbed water in ethanol dehydration on alumina. In Ipatiev's concept, there are no free adsorption surface sites in the reaction cycle, as the exchange of the adsorbed product by the gaseous reactant on the surface site proceeds via a concerted bimolecular substitution (Eqs. (II) and (III)). This adsorption mechanism has been supported by the results of Sadovnikov and Gefter (3, 4), Rozovskii and co-workers (5, 6), and also by our own observations (7–14). Rozovskii (6) has pointed out that displacement adsorption is not limited only to oxides but proceeds even on metal catalysts. The combination of Ipatiev adsorption with Hinshelwood's assumption of a rate-determining step leads to a steady-state kinetic model, called here the Ipatiev–Hinshelwood model by analogy with the widely used Langmuir–Hinshelwood system (1).

Inhibition of the reaction rate by an educt

(Eq. (V)), observed in alkene formation from low alcohols (7–9, 11–14), has been demonstrated also in the cases of deamination of aliphatic amines on alumina (15, 16) and of addition of acetic acid to ethylene on sulfated silica (17).

Transient kinetic data provide more information concerning the mechanism and/or the kinetic scheme than steady-state data, particularly if the reaction scheme is a complex one (17–19), and they can be used as a powerful tool to verify a proposed mechanism.

The first aim of this study was to support the alkoxide mechanism of alkene formation from low aliphatic alcohols proposed earlier (7–13), by a comparison of the most important features of simulated steady-state and transient data in a CSTR with those of the experimental ones.

The second objective was to compare the steady-state kinetic data ( $r - p_A$ ) simulated by the Ipatiev–Hinshelwood model with those provided by the dynamic model, which is not limited by the approximation of the rate-determining step.

## NOMENCLATURE

**A** Reactant (alcohol)  
 $A_p$  Amplitude of molar fraction (–)  
**As, AsA, AsB, and Bs** Adsorbed species

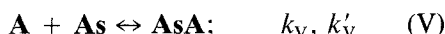
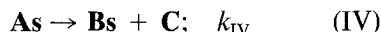
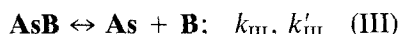
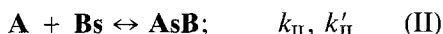
<b>B, C</b>	Products (water and alkene, respectively)
$F, F_A$	Total and alcohol molar flow rate ( $\text{mmol s}^{-1}$ )
H	Hydrogen
I	Inert gas
K	Equilibrium constant of reaction $X + Y_s = X_s Y$ ( $\text{bar}^{-1}$ )
$k, k'$	Rate constants of individual steps ( $\text{s}^{-1}, \text{bar}^{-1} \text{s}^{-1}$ )
M	Metal ion in catalyst surface
O	Oxygen ion in catalyst surface
$p$	Total pressure (bar)
$p_i$	Partial pressure of $i$ th compound (bar)
R	Alkyl
$r$	Steady-state reaction rate ( $\text{mmol (g s)}^{-1}$ )
$r_i$	Reaction rate of $i$ th step ( $\text{s}^{-1}$ )
s	Symbol of active site
$s$	Concentration of active sites ( $\text{mmol g}^{-1}$ )
$t$	Time (s)
$T_l$	Laboratory temperature (K)
$T_r$	Reaction temperature (K)
$T_p$	Period of pulse (s)
$V_0$	Molar volume at $T_r$ and $p$ ( $\text{ml mol}^{-1}$ )
$V_f$	Flow rate of the reaction mixture at $T$ and $p$ ( $\text{ml s}^{-1}$ )
$V_r$	Free volume of the reactor (ml)
$W$	Weight of catalyst (g)
$x, x_i$	Molar fraction of gaseous component or conversion of <b>A</b> (-)
$x_{i,0}$	Input molar fraction of $i$ th compound (-)
$\Phi$	Relative molar feed rate ( $\text{s}^{-1}$ )
$\tau$	Relative molar capacity of reactor (-)
$\Theta$	Molar fraction of adsorbed species on the surface (-)
ss	Steady-state conditions
(X)	Surface concentration of species $X$ ( $\text{mmol g}^{-1}$ )
'	Time derivative ( $\text{s}^{-1}$ )
$^0$	Initial conditions

## THEORETICAL

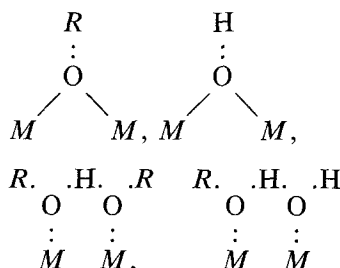
## Reaction Scheme

The simplified reaction scheme of the dehydration of an alcohol (**A**) to water (**B**) and

alkene (**C**) (Eq. (I)) on alumina, based on very detailed information on the reaction mechanism at the molecular level reached in our previous observations (7-13), is expressed by steps (II)-(V):



The species  $\mathbf{A}_s$ ,  $\mathbf{B}_s$ ,  $\mathbf{A}_s\mathbf{A}$ , and  $\mathbf{A}_s\mathbf{B}$  are assumed to be



respectively (8, 12, 13). Only one of them is the active complex reacting directly to alkene, the bridged alkoxide  $\mathbf{A}_s$ . Its decomposition (step (IV)) is the slowest step. Ipatiev adsorption proceeds via steps (II) and (III); the reverse step (III) produces inhibition by the product **B** (water). Step (V) causes the inhibition by the educt. The species  $\mathbf{A}_s\mathbf{B}$  and  $\mathbf{A}_s\mathbf{A}$  are considered to be inactive for direct alkene formation.

## Numerical Simulation

*Steady-state kinetics.* Kinetic equation (1) (Appendix) is based on Ipatiev adsorption (steps (II) and (III)) and Hinshelwood's approximation of a rate-determining step (IV).

$r =$

$$r = \frac{k_{\text{IV}} s K_{\text{AB}} p_{\text{A}}}{K_{\text{AB}} p_{\text{A}} + K_{\text{AB}} K_{\text{BA}} p_{\text{A}} p_{\text{B}} + K_{\text{AA}} K_{\text{AB}} (p_{\text{A}})^2 + K_{\text{BA}} p_{\text{B}}} \quad (1)$$

It is evident that both the product **B** and the educt **A** inhibit the reaction. For  $p_{\text{A}}$  decreasing to zero and  $p_{\text{B}} = 0$ , the equation loses meaning as the limit rate has a finite value ( $r = k_{\text{IV}} s$ ).

**Dynamic model.** Mass action kinetics (Eqs. (2)–(5)) and the approximation of the constant total molar flow were applied in the dynamic model (Eqs. (6)–(12)). Its steady-state solutions (zero left sides) is directly comparable with Eq. (1).

$$r_{II} = p k_{II} x_1 \Theta_5 - k'_{II} \Theta_7 \quad (2)$$

$$r_{III} = k_{III} \Theta_7 - p k'_{III} x_2 \Theta_4 \quad (3)$$

$$r_{IV} = k_{IV} \Theta_4 - p k'_{IV} x_3 \Theta_5 \quad (4)$$

$$r_V = p k_V x_1 \Theta_4 - p k'_V \Theta_6 \quad (5)$$

$$x'_1 = \Phi (x_{1,0}(t) - x_1) - (r_{II} + r_V)/\tau \quad (6)$$

$$x'_2 = \Phi (x_{2,0}(t) - x_2) + r_{III}/\tau \quad (7)$$

$$x'_3 = \Phi (-x_3) + r_{IV}/\tau \quad (8)$$

$$\Theta'_4 = r_{III} - r_{IV} - r_V \quad (9)$$

$$\Theta'_5 = -r_{II} + r_{IV} \quad (10)$$

$$\Theta'_6 = r_V \quad (11)$$

$$\Theta'_7 = r_{II} - r_{III} \quad (12)$$

Numerical indices of molar fractions,  $x_i$  and  $\Theta_i$ , in the kinetic equations (2)–(5),  $i = 1-7$ , correspond to the species **A**, **B**, **C**, **As**, **Bs**, **AsA**, and **AsB**, respectively.  $\Phi = V_f/V_r$  ( $s^{-1}$ ) is the relative feed rate,  $\tau = V_r/(V_0 W s)$  ( $-$ ) is the relative molar capacity of reactor per mol of active sites, and  $x'_i$  and  $\Theta'_i$  ( $s^{-1}$ ) are time derivatives of molar fractions of gaseous and adsorbed components, respectively. The parameters of the reaction system used in the simulations correspond approximately to the real ones:  $V_f = 0.5$  ml  $s^{-1}$  at  $T_1 = 300$  K and  $p = 1$  bar,  $T_r = 450$  K,  $V_r = 0.75$  ml,  $W = 0.058$  g,  $s = 0.350$  mmol  $g^{-1}$ . The rate constants  $k_i$  were selected to obtain qualitative accord between the simulated and the experimental data; they are summarized in Table 1. The input concentration shapes  $x_{i,0}(t)$  are shown in Table 2.

TABLE 1

The Rate Constants ( $s^{-1}$ ,  $bar^{-1} s^{-1}$ ) Used

Step	II	III	IV	V
$k$	5	1	0.05	10
$k'$	0.5	10	0	1

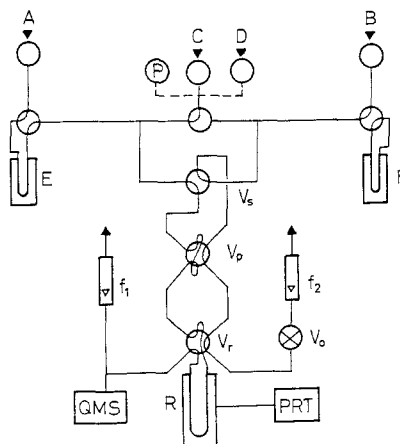


FIG. 1. Experimental setup. (A–D) Gaseous reactants; (E, F) liquid reactant (saturator); ( $V_6$ ) four-way valve for “CHANGE X|Y”; ( $V_p$ ) six-way valve for “PULSE X|Y”; ( $V_r$ ) six-way valve with reactor in the loop; (P) manometer; ( $V_0$ ) pressure control valve; (R) U-tube reactor (i.d. 2 mm); (PRT) temperature programmer; (QMS) quadrupole mass spectrometer.

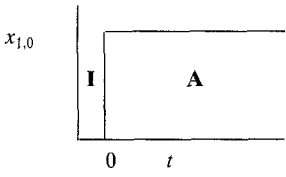
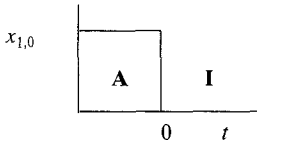
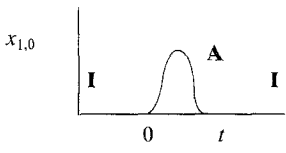
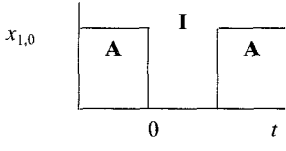
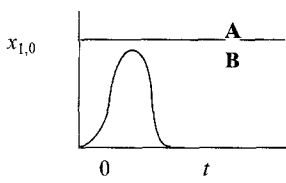
## EXPERIMENTAL

Experimental data to be compared with the simulated ones were obtained previously (11) with the use of GC analysis, and they have been complemented now by a new set of data (denoted as QMS). The experimental setup (Fig. 1) was equipped with a quadrupole mass spectrometer (QMS 420 Balzers) for continuous on-line analysis of the gas reaction mixture. The main fragments were: 45, 41, 18 mass units for propan-2-ol, propene, and water, respectively. The intensity data were converted into concentrations using one-point calibration. The catalyst was alumina (8) of grain size 0.16–0.25 mm. Propan-2-ol p.a. (Lachema Brno) was dried by a molecular sieve. He or  $N_2$  (0.5 ml/s at 300 K, 1 bar) was used as the carrier gas, and the reaction temperature was 450 K.

## RESULTS AND DISCUSSION

The approach to the data treatment and parameter estimation should be described first. It has often been pointed out (e.g. Refs. (20, 21)) that the choice of a kinetic model

TABLE 2  
Shape of Input Perturbations Used in Simulation

Notation	Shape	Function	Initial conditions
CHANGE I A		$t \leq 0, x_{1,0} = 0$ $t > 0, x_{1,0} = 0.25$	$t = 0, x_i^0 = 0,$ $\Theta_i^0 = 0, \Theta_3^0 = 1$ Fresh surface
CHANGE A I		$t \leq 0, x_{1,0} = 0.25$ $t > 0, x_{1,0} = 0$	$t = 0, x_i^0 = x_i^{ss}$ $\Theta_i^0 = \Theta_i^{ss}$ Steady state
PULSE I A		$0 \geq t \geq T_p$ $x_{1,0} = A_p(1 - \cos(2\pi t/T_p))$ $A_p = 0.25, T = 5 \text{ s}$	Fresh surface
PULSE A I		$x_{1,0} = 0.25;$ for $0 \leq t \leq T_p$ $x_{1,0} = 0$ $T_p = 5 \text{ s}$	Steady state
PULSE A B		$x_{1,0} = 0.25$ $x_{2,0} = A_p(1 - \cos(2\pi t/T_p))$ $A_p = 0.25, T = 5 \text{ s}$	Steady state

based exclusively on a quantitative fitting of experimental data may lead to a formal model, with no relation to the real reaction mechanism. The same is valid also in the case of non-steady-state kinetics. Some reasons for such failing of the selection in this case can be: (a) the real system is more complicated than the kinetic model takes into account; the model neglects, for example, the adsorption enthalpy effects, the influence of the reaction mixture on the surface, the transport phenomena, and the minor concurrent surface reactions, (b) a formal model may provide an even better fit

than the realistic (nonformal) model can, and moreover, due to its high flexibility, an infinite number of the parameter sets can produce a suitable fit of the experimental data.

On the other hand, significant support to the model constructed on the basis of independent information on reaction mechanism can provide multiple qualitative correlations of the broad series of the dynamic and steady-state experimental data.

#### Steady-State Kinetics

Figure 2 presents three dependences of reaction rate on the initial partial pressure

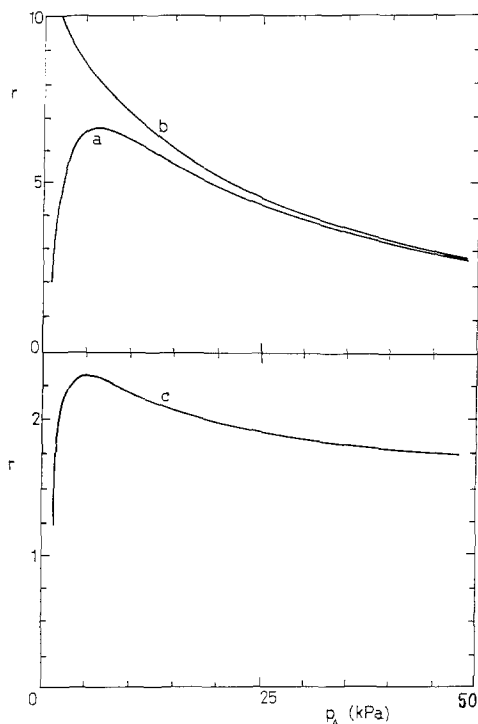


FIG. 2. Reaction rate ( $\text{mmol (g s)}^{-1}$ ) vs  $p_A$ : (a) simulated by the dynamic model Eqs. (6)–(12), (b) calculated according to the Ipatiev–Hinshelwood steady-state model Eq. (1) both for  $W/F_A = 50 \text{ g s mmol}^{-1}$  and (c) experimental (for **A** = ethanol (14)).

of **A**. Figure 2a is simulated by the dynamic model Eqs. (6)–(12); Fig. 2b is calculated according to the Ipatiev–Hinshelwood steady-state kinetic equation (1), respectively, and Fig. 2c is the experimental curve (14) (c.f. (22)). The shape of curves 2a and 2c are similar and the positions of the maxima as well as the limits of reaction rate for partial pressure decreasing to zero and rising to the saturation roughly coincide. In contrast, curve 2b significantly differs from curves 2a and 2c at low partial pressures as the assumption of the rate-determining step being the surface reaction become obviously unrealistic in this concentration region (cf. (21)). On the other hand, good agreement of both curves at higher partial pressures of **A** (40 kPa) demonstrates acceptability of the simple Ipatiev–Hinshel-

wood kinetic model from the practical point of view.

To estimate the influence of reaction time ( $W/F_A$ ) on the shape of the reaction isotherm  $r - p_A$  comparable simulations were performed for three different finite values of  $W/F_A$  (see Fig. 3). (Curve 1 on this figure represents the limit of the Ipatiev–Hinshelwood model for reaction time decreasing to zero). Increasing reaction time leads to a lowering and shifting of the maximum of reaction isotherm to higher  $p_A$ . This effect is caused by the inhibition of the reaction rate by product **B**. To better clarify this influence, further calculations have been made with product **B** in the feed. Figure 4 (curves 2–5) illustrates the situation at  $W/F_A = 5 \text{ g s/mmol}$  for  $p_B = 1, 5, 10,$  and  $50 \text{ kPa}$ . The shapes of the corresponding curves, simulated by the steady-state model (1) and by the dynamic one (Eqs. (6)–(12)), approach with increasing  $p_B$ , showing again the relevance of the Ipatiev–Hinshelwood model.

### Reaction Dynamics

Good qualitative accord of simulated (a) and experimental (b) data has been achieved in all the dynamic experiments (Figs. 5–9).

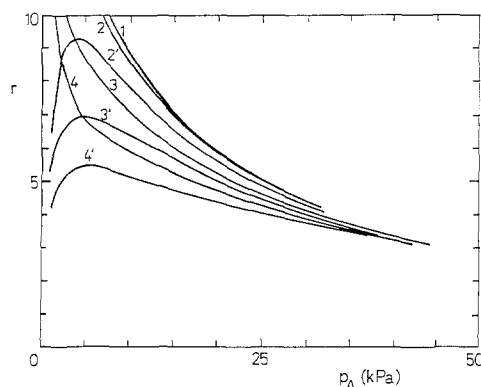


FIG. 3. Reaction rates ( $\text{mmol (g s)}^{-1}$ ) vs  $p_A$ . Curves 1, 2, 3, and 4 are calculated according to Eq. (1) for  $W/F_A = 0.1, 5, 50,$  and  $100 \text{ g s mmol}^{-1}$  respectively; curves 2', 3', and 4' are simulated by dynamic model (Eqs. (6)–(12)) for corresponding  $W/F_A$ .

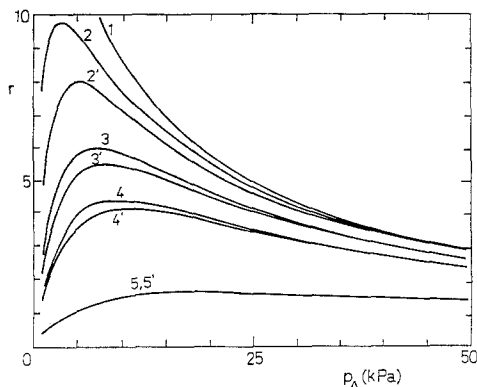


FIG. 4. Reaction rates ( $\text{mmol (g s)}^{-1}$ ) vs  $p_A$ . Curves 1, 2, 3, 4, and 5 are calculated by Eq. (1) for  $W/F_A = 5 \text{ g s mmol}^{-1}$  and  $p_B = 0, 1, 5, 10$  and  $50 \text{ kPa}$  respectively; curves 2', 3', 4', and 5' are simulated for corresponding conditions by dynamic model Eqs. (6)–(12).

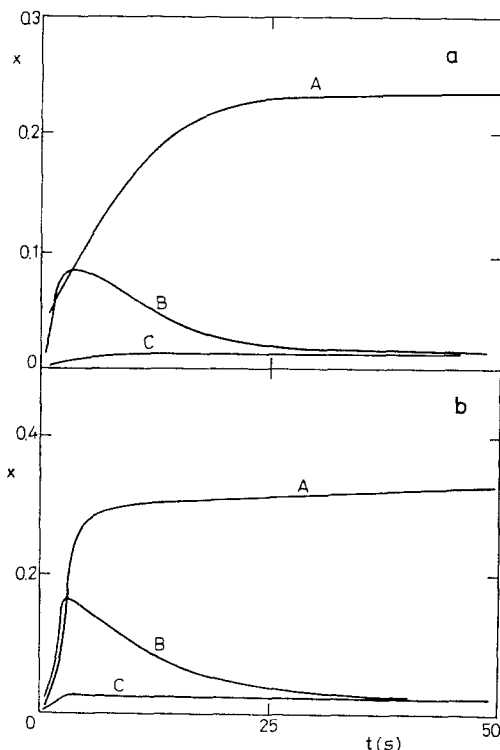


FIG. 5. "CHANGE I|A". (a) Simulated, (b) experimental (QMS) data ( $W = 0.032 \text{ g}$ ,  $V_f = 0.5 \text{ ml s}^{-1}$  ( $T_f, p$ ),  $T_r = 450 \text{ K}$ ,  $x^{ss} = 0.38$ ; A = alcohol, B = water, C = alkene; I = inert gas).

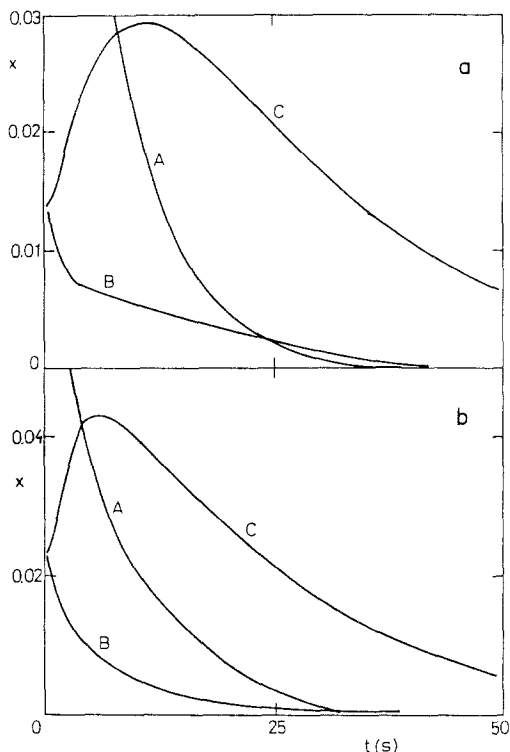


FIG. 6. "CHANGE A|I". (a) Simulated, (b) experimental (QMS) data (for experimental conditions see Fig. 5).

With "CHANGE I|A" (Fig. 5), the concentration jump of A from zero to  $p_A^0$  provokes the typical response of reaction system. In simulation only the Ipatiev displaced adsorption mechanism was considered, and it caused the maximum of concentration of B.

"CHANGE A|I" (Fig. 6) symbolizes a concentration jump of A inverse to the previous one, from a finite value to zero. The broad maximum of C at about 12 s demonstrates the educt inhibition, as can be proven by setting the educt inhibition rate constant  $k_V$  to zero. In such a case, no concentration maximum of C can be observed. Good qualitative agreement between the simulation and the experimental data demonstrates that the description of the educt inhibition kinetics by the dynamic model is adequate.

"PULSE I|A" (Fig. 7) consists of a rapid

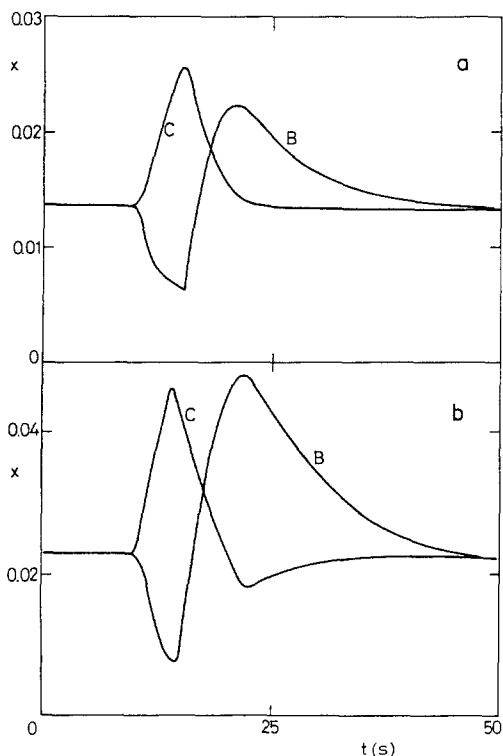


Fig. 7. "PULSE A|I". (a) Simulated, (b) experimental (QMS) data (for experimental conditions see Fig. 5).

sequence of changes  $A|I$  and  $I|A$ , and therefore the response of the reaction system includes typical features of both the preceding ones: the maximum in the concentration of **C**, which coincides with the minimum of **B**, followed by the maximum of **B**. In the real system an inhibiting effect of the product **B** is more pronounced than in the model system, and causes a minimum in the curve of **C**, not observed on the simulated curve.

"PULSE  $I|A$ ": the pulse of **A** introduced into the stream of inert gas provokes the response of the reaction system demonstrated in Fig. 8. The first two compounds leaving the reactor together are the educt **A**, and the product **B**, initially covering the surface, which is displaced from it by **A**. The second nonadsorbing product **C** follows with some delay, as the rate of surface reaction is much lower than that of the other

steps. Some disagreement in the position of the maximum of **C** may arise from the difference in the rate constants of desorption of the inhibiting molecules **A** as well as the surface reaction in the model and the real reaction system.

"PULSE  $A|B$ ": the pulse of strongly adsorbed **B** into steady stream of **A** provokes a typical response (see Fig. 9), which illustrates again the mutual displacement of **A** and **B** by Ipatiev mechanism, as well as the inhibition by product **B**. The minimum on curve **A** is induced by the readsorption of **A** from the feed after temporary occupation of the surface by the product **B**.

#### CONCLUSIONS

The dynamic model (6)–(12) based on the reaction scheme (II)–(V) simulates success-

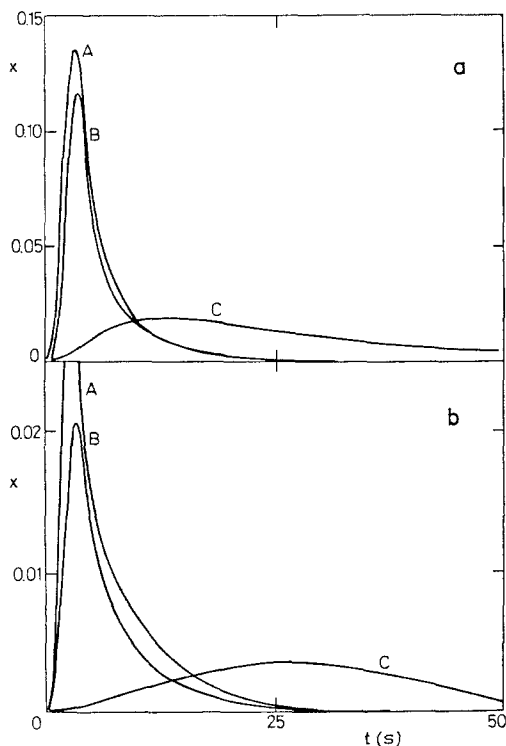


Fig. 8. "PULSE  $I|A$ ". (a) Simulated, (b) experimental data (QMS) (pulse **A** 35 mmol; for experimental conditions see Fig. 5).

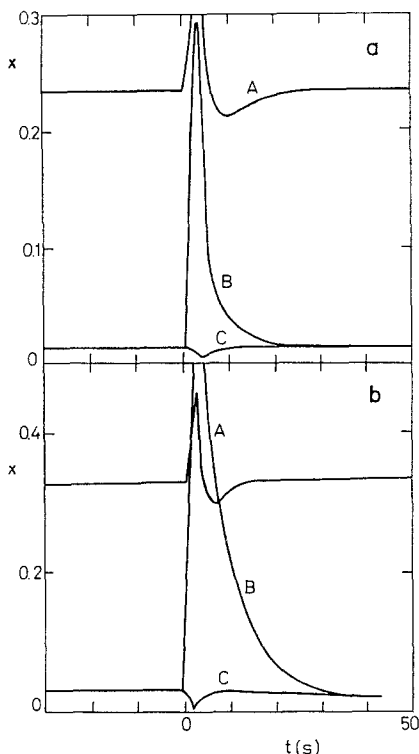


FIG. 9. "PULSE A|B". (a) Simulated, (b) experimental data (pulse B, 70 mmol, for experimental conditions see Fig. 5).

fully the steady state and the transient behavior of the dehydration of a low alcohol (reaction (I)) on alumina in a CSTR. This supports again the previously proposed mechanism of alkene formation from low aliphatic alcohols.

The Ipatiev–Hinshelwood kinetic model (1) provides a realistic prediction of the kinetic data,  $r - p_A$  being in close agreement with that of the dynamic model under the influence of water in the feed and/or higher alcohol pressures.

#### APPENDIX: IPATIEV–HINSHELWOOD KINETIC MODEL

The equilibrium coefficients of reaction (II), inverse reaction (III), and reaction (V) are written as

$$K_{AB} = k_{II}/k'_{II} = (\mathbf{AsB})/p_A (\mathbf{Bs})$$

$$K_{BA} = k'_{III}/k_{III} = (\mathbf{AsB})/p_B (\mathbf{As}) \quad (\text{A-1})$$

$$K_{AA} = k_V/k'_V = (\mathbf{AsA})/p_A (\mathbf{As}).$$

The rate of the slowest step (IV) is expressed as

$$r = k_{IV} (\mathbf{As}). \quad (\text{A-2})$$

Assumptions of saturated surface [ $(s) = 0$ ], low conversion [ $(\mathbf{BsB}) = 0$ ], and symmetry of surface species [ $(\mathbf{AsB}) = (\mathbf{BsA})$ ] lead to a simplified balance equation of the active sites

$$s = (\mathbf{As}) + (\mathbf{Bs}) + (\mathbf{AsA}) + (\mathbf{AsB}). \quad (\text{A-3})$$

Equation (1) follows from Eqs. (A-2), (A-3), and (A-1).

#### ACKNOWLEDGMENTS

Thanks are due to Professors Miloš Kraus and Petr Schneider for the support and helpful discussion of all problems.

#### REFERENCES

1. Yang, K. H., and Hougen, O. A., *Chem. Eng. Prog.* **146** (1950).
2. Ipatiev, V. N., "Catalytic Reaction at High Pressures and Temperatures." Macmillan, New York, 1936.
3. Sadovnikov, V. V., and Geftter, A. M., *Izv. Akad. Nauk SSSR Ser. Khim.* **1220** (1976).
4. Sadovnikov, V. V., and Geftter, A. M., *React. Kinet. Catal. Lett.* **6**, 415 (1977).
5. Rozovskii, A. Ya., Vitnova, L. A., Tretiakov, G., Lin, A. M., and Yaniukova, L. M., *Kinet. Katal.* **23**, 1401 (1982).
6. Rozovskii, A. Ya., *Kinet. Katal.* **30**, 533 (1989).
7. Morávek, V., Ph.D. thesis, Czechoslov. Acad. Sci., Prague, 1983.
8. Morávek, V., and Kraus, M., *J. Catal.* **87**, 452 (1984).
9. Morávek, V., *React. Kinet. Catal. Lett.* **30**, 71 (1986).
10. Malysheva, L. V., Morávek, V., Paukshtis, E. A., and Yurchenko, E. N., *Collect. Czech. Chem. Commun.* **53**, 743 (1988).
11. Morávek, V., and Kraus, M., *Collect. Czech. Chem. Commun.* **50**, 1168 (1985).
12. Morávek, V., Lamotte, J., and Lavalley, J.-C., in "Proceedings, 6th Int. Symp. Heter. Catalysis, Sofia, 1987," Part i, p. 377.
13. Lamotte, J., Lavalley, J.-C., and Morávek, V., *Kinet. Catal. Lett.* **40**, 25 (1989).



14. Morávek, V., and Kraus, M., *Collect. Czech. Chem. Commun.* **51**, 763 (1986).
15. Hogan, P., Ph.D. thesis, Inst. Chem. Technol., Prague, 1970.
16. Koubek, J., Ph.D. thesis, Inst. Chem. Technol., Prague, 1974.
17. Truffer, M. A., and Renken, A., *AIChE J.* **32**, 1612 (1986).
18. Hofmann, H., *Dechema Monogr.* **120**, 31 (1989).
19. Klusáček, K., Hudgins, R. R., and Silveston, P. L., *Can. J. Chem. Eng.* **67**, 516 (1989).
20. Morávek, V., Duchet J.-C. and Cornet, D., *Appl. Catal.* **66**, 257 (1990).
21. Morávek, V., and Sadovnikov, V. V., *React. Kinet. Catal. Lett.* **37**, 357 (1988).
22. Krampera, F., and Beránek, L., *Collect. Czech. Chem. Commun.* **51**, 774 (1986).